A Study of Cross-Width Variations in the Two-Dimensional Foil Bearing Problem

Sinan Müftü [1]
Post-Doctoral Research Associate.

Richard C. Benson
Professor and Chair.

Mechanics of Flexible Structures Project,
Department of Mechanical Engineering,
University of Rochester,
Rochester, NY 14627

The foil bearing problem, common to magnetic tape recording, is modeled through numerical simulation. The emphasis is on the effects of cross-width changes in the system parameters. Air lubrication is modeled using the Reynolds equation including the first-order slip correction terms and compressibility. A segmented structural model is introduced for the tape displacements where the tape is modeled as a cylindrical shell in the wrap zone and as a plate in the straight segments between the guide pins and the tangency points. Tape inertia and transport effects are included by using the material time derivative of the displacements. An explicit time integration method is used for the tape equation in order to obtain a faster transient coupling algorithm. The Reynolds equation is solved with the alternating direction implicit (ADI) integration method. The effects of axial tape tension, guide shape variations and the tape width on the steady-state tape-guide separation are investigated. It is shown that small axial variations on the parameters mentioned can lead to important and unintended variations in tape-guide separation.

1 Introduction

In this paper, we present a fully coupled, transient, numerical solution to the finite width (2-D) foil bearing problem encountered in magnetic tape recording, and we study the effects of cross-width variations on the steady-state tape-guide separation. Study of the width effects is motivated by several reasons. Imperfections in a tape system's parameters, such as axial tension variations, cause cross-tape asymmetry. In linear recording, increasing demands on increasing the bit density will eventually necessitate the use of unused bands on the sides of the tape. These bands can not be modeled by assuming that the foil bearing is infinitely wide (1-D). Continuing trends to use smaller form factors in recording will hasten the emergence of narrower tapes for linear recording. However, as the tape is made narrower the displacement boundary layers on the free edges of the tape merge.[2] This can not be modeled by a 1-D analysis, either. In helical scan recording there is no longitudinal symmetry, therefore, the analysis of this type of recording should consider the width effects.

In modeling the finite width foil bearing problem, past investigators have used various formulations. Two common, simplifying assumptions have been that the air is incompressible, and that slip flow may be ignored. Compressibility and slip flow are kept in our lubrication equation because they are important for the range of flying heights we would like to model.

A variety of equations have been used to model the tape. Barlow (1967), Wolf et al. (1983), Heinrich and Connolly (1992), Lacey (1992), and Mizoh et al. (1992) consider only the out-of-plane displacement, w, in the derivation of the equation of equilibrium whereas Greenberg (1979), Yoneda and Sawada (1988), Fujimoto et al. (1993), and Kotera et al. (1993) consider also the in-plane displacements u and v. Except for Wolf et al., all of these studies consider the bending stiffness of the tape. The orthotropy of the tape is considered by Mizoh et al. (1992). In establishing strain-displacement relations Barlow, Greenberg, Mizoh et al., and Kotera use linear relationships and Fujimoto and Rongen (1990) consider the nonlinear terms. The linear strain-displacement assumption is suitable for modeling longitudinal recording, whereas nonlinear strain-displacement relations and in-plane displacements should be employed in modeling helical scan recording where the head penetration causes large rotations, and friction forces cause in-plane loading. In this study, we consider isotropic bending stiffness, small displacement, and rotations of the tape and we neglect the in-plane displacements u and v.

2 Tape Geometry

The tape is wrapped around a cylindrical guide for a large angle and is supported by two pins on the left and right side of the guide as shown in Fig. 1. In order to reduce the computational effort required to solve the problem we assumed that the support pins are moved closer to the tangency points between the tape and the guide as shown in detail A of Fig. 1. This idea was first used by Granzow and Lebeck (1985), and it was shown that it does not affect the steady state tape-guide separation. The total tape length between the moved pins is L_x and the width of the tape is L_y. As we want to analyze arbitrarily large wrap angles we used a segmented model for the tape equation. In this model, the reference configuration for the tape in the *wrap zone* is the cylindrical surface of the guide. In the *entry* and *exit zones* the reference configuration is the flat surfaces connecting the tangency points to the pins. When a Cartesian coordinate system is placed on the left-hand side pin the entry zone is given in $0 \le x \le L_{x1}$, the wrap zone is given in $L_{x1} \le x \le L_{x2}$, and exit zone is given in $L_{x2} \le x \le L_x$. The distance between the moved supports and the reference configuration of the tape in the entry and exit zones becomes w_L and w_R, respectively, as shown in Fig. 1. We neglect the in-plane displacements. The displacements w_L and w_R affect the simple support boundary condition for the tape given below.

The distance between the undeflected tape and the guide is denoted by $\delta(x, y)$. The x direction variation of this function,

[1] Current address: MIT Haystack Observatory, Westford, MA 01886.

[2] See Fung and Wittrick (1955) for more on the displacement boundary layers in thin bent plates.

Contributed by the Tribology Division for publication in the JOURNAL OF TRIBOLOGY. Manuscript received by the Tribology Division June 16, 1994; revised manuscript received April 3, 1995. Associate Technical Editor: D. E. Brewe.

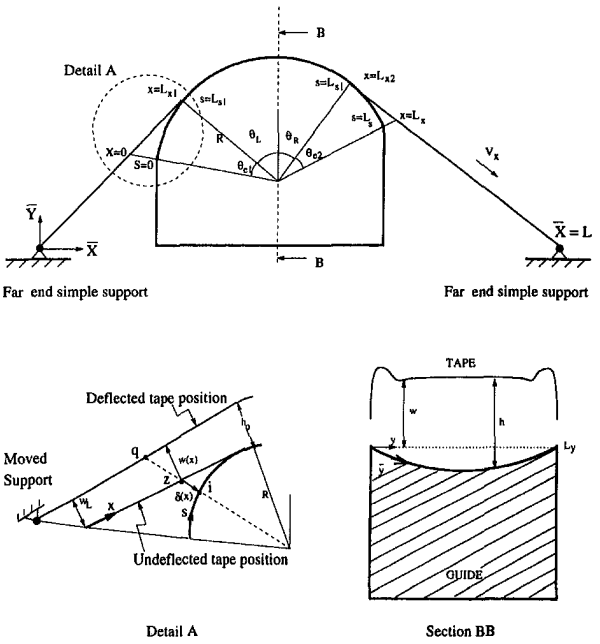

Fig. 1 Tape geometry for the large angle of wrap analysis. Shown are the undeflected (reference) and deflected shapes.

$\delta_x(x)$, is calculated in the $(\bar{X}, \bar{Y})$ coordinate system shown in Fig. 1, and it is given as follows:

$$\delta_x(x) = \begin{cases} \sqrt{(\bar{X}_i - \bar{X}_z)^2 + (\bar{Y}_i - \bar{Y}_z)^2}, & 0 \le x \le L_{x1} \\ 0 & L_{x1} \le x \le L_{x2} \\ \sqrt{(\bar{X}_i - \bar{X}_z)^2 + (\bar{Y}_i - \bar{Y}_z)^2}, & L_{x2} \le x \le L_x \end{cases} \quad (1)$$

See Fig. 1 for the locations of points i and z. In the 2-D foil bearing problem we allow for a half-sine wave variation on the guide surface in the axial direction, as shown in section BB in Fig. 1. Thus $\delta(x, y)$ becomes,

$$\delta(x, y) = \delta_x(x) + A \sin\left(\frac{\pi y}{L_y}\right) \quad (2)$$

where A is the amplitude of the surface shape, and its value is positive when a dented surface is modeled and negative when a surface with a protrusion is modeled. Unless otherwise stated, all of the cases studied in this paper assume a flat guide surface, without any axial variation.

3 Governing Equations

The equation of motion for the out-of-plane displacements, w, of a thin elastic tape with thickness, c, and bending stiffness, D, is similar to the equation of motion of a cylindrical shell (Müftü and Benson, 1994a)

$$D\nabla^4 w + Kw - T_x \frac{\partial^2 w}{\partial x^2} + \rho_a\left(V_x^2 \frac{\partial^2 w}{\partial x^2} + 2V_x \frac{\partial^2 w}{\partial x \partial t} + \frac{\partial^2 w}{\partial t^2}\right) = p + P_c - P_a - P_{BW} \quad (3)$$

In this equation x is the circumferential direction, y is the axial direction, and t is time. The segmented nature of this equation comes from the shell stiffness, K, and the belt wrap pressure, P_{BW}, terms which are given as follows,

$$K = \begin{cases} 0, & 0 \le x \le L_{x1} \\ \dfrac{Ec}{R^2(1-\nu^2)}, & L_{x1} \le x \le L_{x2} \\ 0, & L_{x2} \le x \le L_x \end{cases} \quad (4)$$

$$P_{BW} = \begin{cases} 0, & 0 \le x \le L_{x1} \\ \dfrac{T_x}{R}, & L_{x1} \le x \le L_{x2} \\ 0, & L_{x2} \le x \le L_x \end{cases} \quad (5)$$

In Eq. (3) the tape is assumed to be under tension, T_x, and moving longitudinally with speed V_x. The loading on the tape is provided by the air pressure, $p - P_a$, the contact pressure, P_c, and the belt wrap pressure. Ambient pressure is P_a. The contact pressure is modeled by the asperity compliance relation given by Lacey (1992),

$$P_c = \begin{cases} \left(\dfrac{\sqrt{P_m}}{\sigma_t}(\sigma_t - h)\right)^2 & \text{if } h \le \sigma_t \\ 0 & \text{if } h \ge \sigma_t \end{cases} \quad (6)$$

where, σ_t, the height of the surface asperities at which contact starts, and P_m, the pressure required to force the tape-guide spacing, h, to zero are two experimentally determined constants. The values of P_m and σ_t for chromium dioxide tape are reported as 4.72 MPa and 93.4 nm, respectively (Lacey, 1992). Alternatively, one may employ a similar contact pressure function given by the Greenwood and Williamson model (Bhushan, 1990).

The pins supporting the tape are modeled as simply-supported boundaries and lateral edges of the tape are modeled as free boundaries. Thus the boundary conditions become,

Simply Supported Boundaries:

$$M_x = D\left[\frac{\partial^2 w}{\partial x^2} + \nu \frac{\partial^2 w}{\partial y^2}\right] = 0$$

$$\text{at} \quad x = 0, L_x, \quad \text{and} \quad 0 \le y \le L_y \quad (7)$$

$$w = w_L \quad \text{at} \quad x = 0, \quad \text{and} \quad 0 \le y \le L_y$$

$$w = w_R \quad \text{at} \quad x = L_x, \quad \text{and} \quad 0 \le y \le L_y \quad (8)$$

Free Boundaries:

$$M_y = D\left[\frac{\partial^2 w}{\partial y^2} + \nu \frac{\partial^2 w}{\partial x^2}\right] = 0,$$

$$\text{at} \quad y = 0, L_y, \quad \text{and} \quad 0 \le x \le L_x \quad (9)$$

$$Q_y^{eq} = D\left[\frac{\partial^3 w}{\partial y^3} + (2-\nu)\frac{\partial^3 w}{\partial x^2 \partial y}\right] = 0,$$

$$\text{at} \quad y = 0, L_y, \quad \text{and} \quad 0 \le x \le L_x \quad (10)$$

where, M_x, M_y, and Q_y^{eq} are the bending moment resultants in x and y directions and the equivalent shear force resultant in

Table 1 Steady-state tape-guide separation values at ($L_x/2$, $L_y/2$) when there is a sinusoidal dent or protrusion on the guide surface

	h [μm]	
A [μm]	Protrusion	Dent
1	0.763	0.806
3	0.725	0.854

Table 2 Specifications for test cases from Stahl et al. (1974) are given on the left-hand side column and from Vogel and Groom (1974) are given on the right-hand side column

N	No. of nodes for tape (y-dir.)	71	71	
M	No. of nodes for tape (x-dir.)	172	172	
N_p	No. of nodes for air bearing (y-dir.)	71	71	
M_p	No. of nodes for air bearing (x-dir.)	172	172	
Δt	Time step size	0.1	0.1	μs
α	Integration parameter	0	0	
β	Integration parameter	1/4	1/4	
γ	Integration parameter	1/2	1/2	
V_x	Tape speed	2.54	1.27	m/s
T_x	Tape tension	278	176.7	N/m
c	Tape thickness	20	38.1	μm
L_x	Tape length (appr.)	15	15	mm
L_w	Tape width	6.35	6.35	mm
E	Young's modulus	4.0	4.0	*GPa*
ρ_a/c	Volumetric mass density of the tape	1400	1400	kg/m^3
ν	Poisson's ratio	0.3	0.35	
R	Guide radius	2.04	2.0	cm
θ_L	Wrap angle (see Fig. 1)	8.89°	5.2734°	
θ_R	Wrap angle	8.89°	5.2734°	
θ_{e1}	Entry angle	12°	16.6654°	
θ_{e2}	Exit angle	12°	16.6654°	
$\bar{L}$	Distance between far end supports	8.44	8.44	cm
P_a	Ambient pressure	84.1	101.3	kPa
μ_a	Air viscosity	1.81×10^{-5}	1.81×10^{-5}	N/m^2 s
λ_a	Mean free path length of air	63.5	63.5	nm

the y direction, respectively. Two initial conditions are required for the transient simulation.

Initial Conditions:

$$\text{Initial displacement,} \quad w(x, y, 0) = w^o(x, y) \tag{11}$$

$$\text{Initial displacement velocity,} \quad \frac{\partial w(x, y, 0)}{\partial t} = v^o(x, y) \tag{12}$$

The initial conditions, w^o, v^o, are defined below by Eq. (17).

The air lubrication is modeled by using the modified Reynolds equation (Hamrock, 1994).

$$\frac{\partial}{\partial s}\left[h^3 p \frac{\partial p}{\partial s}\left(1 + 6\frac{\lambda_a}{h}\right)\right] + \frac{\partial}{\partial \bar{y}}\left[h^3 p \frac{\partial p}{\partial \bar{y}}\left(1 + 6\frac{\lambda_a}{h}\right)\right] = 12\mu_a \frac{\partial ph}{\partial t} + 6\mu_a(V_x + V_x^G)\frac{\partial ph}{\partial s} + 6\mu_a(V_y + V_y^G)\frac{\partial ph}{\partial \bar{y}} \tag{13}$$

where, p, is the air pressure, h, is the tape-guide separation, λ_a, is the molecular mean free path length of air, μ_a is the viscosity of air, and s and $\bar{y}$ are the spatial coordinates on the guide surface in the circumferential and axial directions, respectively. Tape velocity components are denoted by V_x and V_y and the guide velocity components are denoted by V_x^G and V_y^G. The boundary conditions and initial condition for the Reynolds equation are,

$$p(0, \bar{y}) = p(L_x, \bar{y}) = p(s, 0) = p(s, L_y) = P_a \tag{14}$$

$$p(s, \bar{y}, 0) = p_o(s, \bar{y}) \tag{15}$$

The tape-guide separation, h, couples the equations governing the two media,

$$h(x, y, t) = w(x, y, t) + \delta(x, y) \tag{16}$$

For the upcoming example problem the following initial conditions are used.

$$w^o(x, y) = w_o^{1D}(x)$$
$$v^o(x, y) = 0 \tag{17}$$
$$p^o(x, y) = P_a + (p_o^{1D}(x) - P_a)\frac{4}{L_y}\left(y - \frac{y^2}{L_y}\right)$$

where, $w_o^{1D}(x)$ denotes the displacement distribution, and $p_o^{1D}(x)$ denotes pressure distribution of the 1-D problem at the steady state (Müftü, 1994b). In order to avoid artificially large gradients in air pressure, which proved to be hard to handle with the numerical integration method, initially we specified a parabolic pressure variation as given in (17). For the example cases of this paper the guide surface is stationary, and the tape moves in the circumferential direction only, therefore V_y, V_y^G, and V_x^G are zero in (13).

4 Solution Method

Governing equations are solved separately by numerical techniques as described below and they are coupled in the transient domain. The details of the numerical method are given by Müftü (1994b). The equation of motion of the tape is discretized in space by using second-order accurate finite difference approximations of the derivatives involved and it is replaced by the following matrix equation,

$$[K]\{w\} + [G]\{v\} + [M]\{a\} = \{F\} \tag{18}$$

where $[K]$ is the stiffness matrix, $[G]$ is the transport matrix, $[M]$ is the inertia matrix, $\{w\}$ is the displacement vector, $\{v\}$ is the velocity vector, and $\{a\}$ is the acceleration vector. After we discretize[3] Eq. (18) in time we denote the "current" time step with the superscript $n + 1$. The forcing vector $\{F^{n+1}\}$ is given in (19) where $\{f_b\}$ is a time-invariant vector which represents the contribution of the constant displacements applied to the moved supports. We used a uniform finite difference mesh where the spacings between discretized points on the tape were equal in both x and y directions. The discretized equation of motion is, then integrated in time by the Hilber-Hughes-Taylor method (Hughes, 1987).

The Reynolds equation is solved by the alternating direction implicit (ADI) method as given by White and Nigam (1980). In this method, Eq. (13) is factored in the x and y directions as given in (21), where $L_x(\ )^n$ and $L_y(\ )^n$ are the finite difference operators, $\{\phi^{n+1}\}$ is the loading vector, and $z = ph$.

The coupled system of equations is nonlinear due to contact and Reynolds equations. Therefore, in the coupling algorithm given below we iterate within a given time step between the

[3] See the coupling algorithm.

solutions of the tape equation and the Reynolds equation. We advance the solution to the next time step only after the iteration criteria are satisfied. The program is stopped after a prespecified number of time steps are executed. In the following coupling algorithm the subscript k refers to the spatial nodal values of the respective vectors. The iteration counter within a time step is i.

1 Initial Conditions:

$$w_k^0 = \bar{w}_k, \quad p_k^0 = \bar{p}_k, \quad v_k^0 = \bar{v}_k, \quad a_k^0 = 0, \quad n = 0 \quad t = \Delta t.$$

2 Predictors:

$$\tilde{w}_k^{n+1} = w_k^n + v_k^n \Delta t + (\tfrac{1}{2} - \beta)\Delta t^2 a_k^n, \quad \tilde{p}_k^{n+1^{(i)}} = p_k^n,$$

$$\tilde{v}_k^{n+1} = v_k^n + (1 - \gamma)\Delta t a_k^n, \quad h_k^n = w_k^n + \delta_k$$

$$\tilde{a}_k^{n+1} = 0, \quad i = 0$$

3 Start Iterations:

$$w_k^{n+1^{(i+1)}} = \tilde{w}_k^{n+1}, \quad p_k^{n+1^{(i+1)}} = \tilde{p}_k^{n+1^{(i)}},$$

$$v_k^{n+1^{(i+1)}} = \tilde{v}_k^{n+1}, \quad h_k^{n+1^{(i+1)}} = h_k^n$$

$$a_k^{n+1^{(i+1)}} = \tilde{a}_k^{n+1}, \quad z_k^n = h_k^n p_k^n$$

4 Calculate P_c, f_{eq}, a^{n+1}:

$$\text{If} \quad h_k^{n+1^{(i+1)}} \le \sigma_t \quad \text{then} \quad P_{c_k}^{(i+1)} = \left(\frac{\sqrt{P_m}}{\sigma_t} (\sigma_t - h_k^{n+1^{(i+1)}}) \right)^2$$

$$F_k^{n+1^{(i+1)}} = p_k^{n+1^{(i+1)}} - Pa - P_{BW_k} + P_{c_k}^{(i+1)} + f_{b_k} \tag{19}$$

$$f_{eq_k} = [(1 + \alpha)F_k^{n+1^{(i+1)}} - \alpha F_k^n - (1 + \alpha) \times (G\tilde{v}_k^{n+1} + K\tilde{w}_k^{n+1}) + \alpha(Gv^{n_k^{(i+1)}} + Kw_k^{n^{(i+1)}})]$$

$$a_k^{n+1^{(i)}} = \frac{f_{eq_k}}{\rho_a} \tag{20}$$

5 Correctors:

$$w_k^{n+1^{(i+1)}} = \tilde{w}_k^{n+1} + \beta \Delta t^2 a_k^{n+1^{(i+1)}}$$

$$v_k^{n+1^{(i+1)}} = \tilde{v}_k^{n+1} + \gamma \Delta t a_k^{n+1^{(i+1)}}$$

$$h_k^{n+1^{(i+1)}} = w_k^{n+1^{(i+1)}} + \delta_k$$

6 Solve for p^{n+1}:

$$[1 - L_x(\ \ )][1 - L_y(\ \ )]\Delta z_k^{n+1} = \phi_k^{n+1} \tag{21}$$

$$z_k^{n+1^{(i+1)}} = z_k^n + \Delta z_k^{n+1} \tag{22}$$

$$p_k^{n+1^{(i+1)}} = z_k^{n+1^{(i+1)}} / h_k^{n+1^{(i+1)}} \tag{23}$$

7 Check for Convergence:

$$\left| \frac{p^{n+1^{(i+1)}} - p^{n+1^{(i)}}}{p^{n+1^{(i)}}} \right| < \epsilon_p \quad \text{and}$$

$$\left| \frac{w^{n+1^{(i+1)}} - w^{n+1^{(i)}}}{w^{n+1^{(i)}}} \right| < \epsilon_w \quad \text{for all} \quad k$$

If no then

$$p_k^{n+1^{(i)}} = p_k^{n+1^{(i+1)}}, \quad i = i + 1 \quad \text{go to} \quad 4$$

If yes then

$$p_k^n = p_k^{n+1^{(i+1)}}, \quad v_k^n = v_k^{n+1^{(i+1)}},$$

$$h_k^n = h_k^{n+1^{(i+1)}}, \quad w_k^n = w_k^{n+1^{(i+1)}},$$

$$a_k^n = a_k^{n+1^{(i+1)}}, \quad n = n + 1,$$

$$t = t + \Delta t,$$

If $t < \tau$ then go to 2

8 Stop

The convergence criteria for the pressure and the displacement, as given in Step 7 of the algorithm, were chosen to be $\epsilon_p = \epsilon_w = 1 \times 10^{-3}$. In this algorithm α, β and γ are the integration constants of the time integration method. The time step size is Δt. In order to find the steady state of a given problem we trace the transient solution to steady state while keeping its parameters constant. To reach a steady-state solution we run the simulation for a duration of $\tau \le 2(L_x/V_x)$ as suggested by Eshel's study (1969) while we also trace the change in displacement as a function of time. The total number of time steps is in the order of $\tau/\Delta t$. Note that in this coupling algorithm we do not need to relax the pressure or the spacing between the time steps. This is in contrast to algorithms in which the equations are coupled in steady state.

The above algorithm is similar to the one given by Heinrich and Connolly (1992). However, we used an explicit time integration technique, in order to decrease the computation time. This is especially important in studying the transient effects of the problem.[4] By using the explicit method the computational burden of the matrix inversion for determining $\{w^{n+1}\}$, necessarily used by the implicit approach (Müftü and Benson, 1994a) is avoided. However, in this case the integration in time is conditionally stable. The stability analysis of the explicit time integration algorithm, available only for $\alpha = 0$ (Hughes, 1987), shows that $\gamma = \frac{1}{2}$ and $\beta = \frac{1}{4}$ provides a second order accurate time integration method.

In a separate study, we analyzed the frequency behavior of the tape equation and showed that the governing equation for the tape displacements is dispersive (Müftü, 1994b). Therefore, the critical frequency of the tape equation does not have a single value, and it is not possible to find a simple relation for the critical time step size. In Müftü (1994b), we also showed that the phase and group velocity errors introduced due to spatial discretization can be reduced by decreasing the spatial step size, Δx $(=\Delta y)$. Our experience shows that, the critical time step size, Δt, determined for the solution of the tape equation is not necessarily the value that would provide a successfully *coupled* solution.

In order to determine the critical value of the time steps for the coupled system, we made numerical experiments, where we monitored the transient response of the system as well as its steady state solution. We determined an upper limit for Δt by employing an implicit version of the tape equation solver (Müftü, 1994b). As the Reynolds equation is also solved implicitly, the solution obtained this way is limited only due to coupling, but not due to the individual equations. For a system whose parameters are similar to the values given in Table 2, this study gave a critical time step of 0.15 μs. We took this value as the upper limit of the numerical experiments to determine the critical time step size for the coupled solution in which explicit solution of the tape equation is used. The coupled solution with the explicit time integration required smaller time steps. Decreasing Δt to 0.1 μs was sufficient for reaching a repeatable steady state solution. At this point it is interesting to note that the critical time step for the implicit solution of the tape equation was not significantly different than the explicit solution. However, we observed that smaller time steps were required for solving a problem in which contact pressures were more significant than the examples presented here.

[4] The authors are currently preparing a paper on the results of the 2-D transient problem.

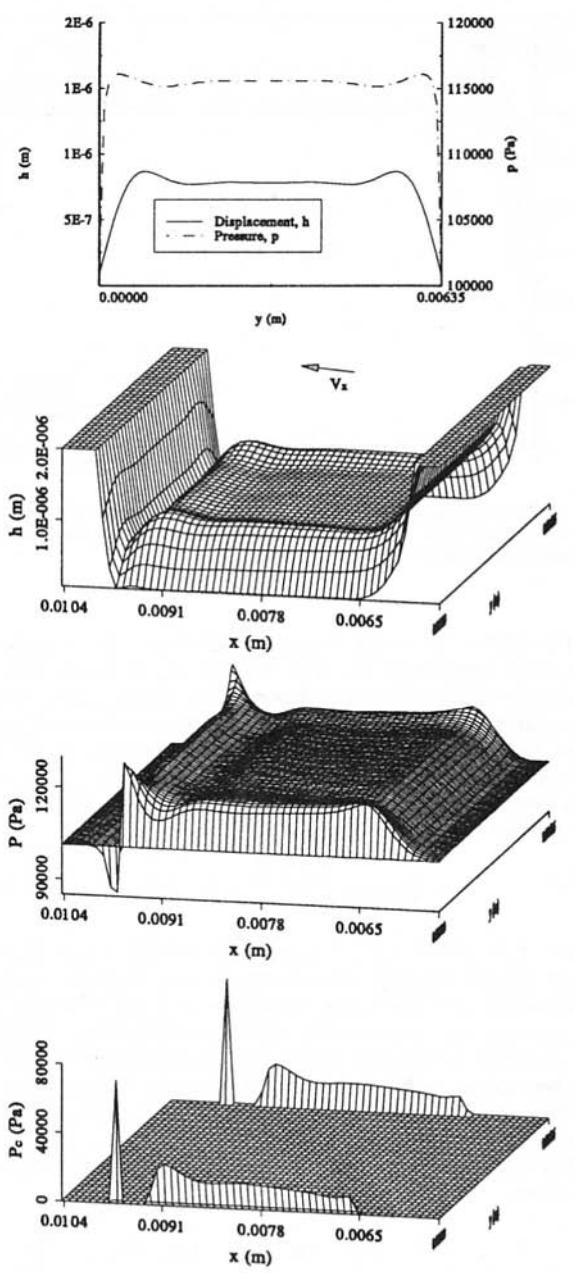

Fig. 2 The tape-guide spacing, h, air pressure, p, and the contact pressure, p_c at steady state. The tape speed and tension are, V_x = 1.27 m/s, and T_x = 276.7 N/m. The mid-point flying height is h_o = 0.785 μm. See the right-hand side column of Table 2 for problem parameters.

5 Results

The Steady State in Linear Recording. The steady state of the tape-guide spacing, h, air pressure p, and contact pressure, P_c for a case whose parameters are given on the right hand side column of Table 2 are presented in Fig. 2. This figure shows that the contact pressure at the free edges of the tape is nonzero. The minimum displacement occurs on the free edges of the exit side of the tape. The presence of the contact pressure makes the sides of a guide most vulnerable locations for wear.

We see that on the lateral edges the air pressure reaches its value in the middle of the tape from the ambient pressure in narrow boundary layers. In these side boundary layers the pressure is largest near the free edges due to lower tape-guide spacing. In Fig. 2 we see another boundary layer at the exit side where the pressure drops to the ambient in an undulating manner. In the exit side boundary layer the air pressure dips below ambient and it shows spikes at the free edges, where the maximum and minimum pressures are located near each other. Mixing of the side and exit pressure boundary layers cause these "corner spikes" in the pressure.

Tape Width Effects in Linear Recording. In Figs. 3–5 we show the effect of tape width on the steady state tape guide spacing, h. The widths considered are, L_y = 2, 4, 8 and 12 mm. Other tape parameters are as indicated in the respective figure captions, and can be found in Table 2. The tape displacement follows the shape of the pressure boundary layers mentioned above. Figure 3 shows that for the 2 mm wide tape, the displacement boundary layers are mixed, and the constant gap region in the width direction is lost. This is better observed in the cross sectional views given in Fig. 5. Looking at the 4 mm wide tape, we see, in Figs. 3 and 5, that the displacement boundary layers are almost separated. For wider tapes, L_y = 6.35 mm in Fig. 2, and L_y = 8 and 12 mm in Figs. 3–5, we see a wider cross-tape constant gap region. Close inspection of Fig. 5 shows that the width of the displacement boundary layer at the sides of the tape is independent of the total tape width, except for the 2 mm case where the two boundary layers are mixed. The width of this displacement boundary layer is approximately 2.5 mm.

In Fig. 6 we show the effects of the tape thickness on the steady state tape-guide separations for c = 5, 10, 20, and 40

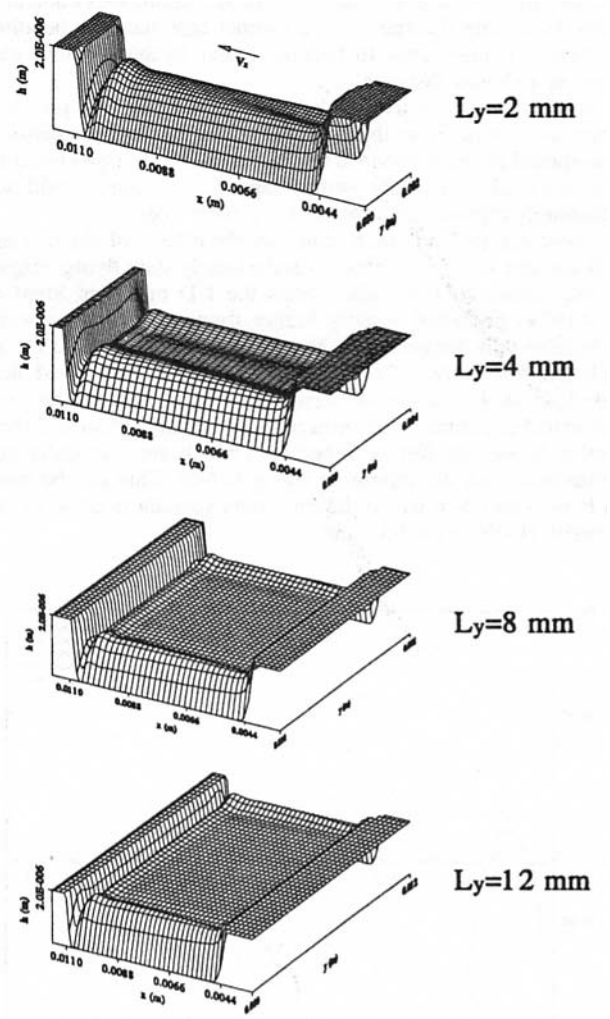

Fig. 3 Steady-state tape-guide spacing, h, for different tape widths, L_y. The mid-point flying heights, h_o, are 1.342, 1.217 and 1.207 μm, respectively. The tape speed and tension are, V_x = 2.54 m/s, and T_x = 278 N/m, tape thickness is c = 20 μm. See the left-hand side column of Table 2 for problem parameters.

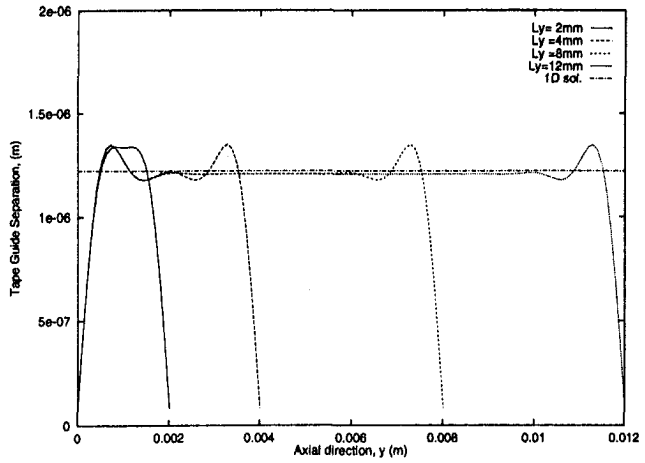

Fig. 4 Cross section of the steady-state tape-guide spacing, h, for different tape widths at $x = L_x/2$. The mid-point flying heights, h_o, are 1.342, 1.217, and 1.207 μm, respectively. See the left-hand side column of Table 2 for problem parameters.

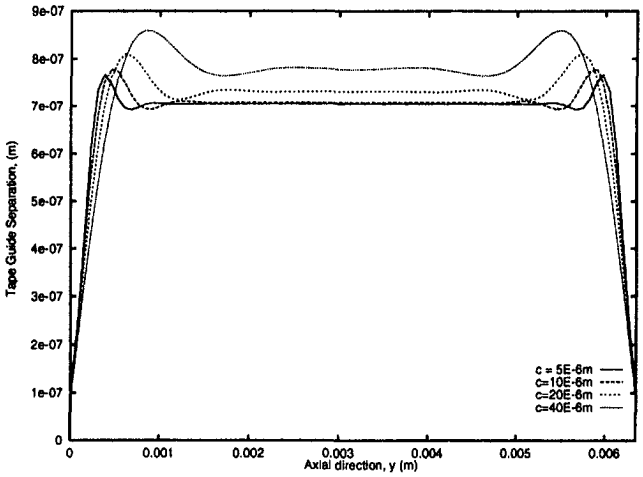

Fig. 6 Tape-guide separation as a function of thickness, c. Cross sections are given at $x = L_x/2$. See the right hand side column of Table 2 for problem parameters.

μm. We see from this figure that the steady-state flying height becomes lower as thinner tapes are used. We also see that the displacement boundary layer becomes narrower. This is due to the fact that the tape's bending resistance diminishes cubically with decreasing thickness. As a thinner tape has less bending resistance it thus tends to become flatter in the constant gap zone in a shorter distance.

Similar observations can be made about the air pressure boundary layers. From these figures we conclude that a distinction should be made between the narrow and wide tapes because the results obtained for a narrow tape, $L_y < 5$ mm, would not adequately represent the results for a wide one.

These results lead one to consider the effects of the side air leakage and surface roughness on the steady state flying height. In the classic back-to-back studies the 1-D model of Stahl et al. (1974) predicted slightly higher flying heights than were experimentally measured by Vogel and Groom (1974). Heinrich and Connolly (1992) in their 2-D study confirmed that side leakage does lower the steady-state flying height. Our own numerical experiments confirm the side leakage effect and they further show that surface asperities (which are elastically deformable) limit the minimum flying height. This can be seen in Figs. 4 and 5 in which the minimum spacing is close to the asperity height, $\sigma_t = 93.4$ nm.

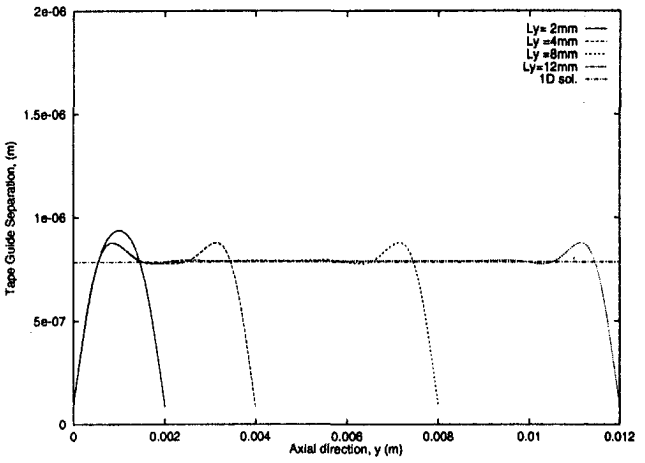

Fig. 5 Cross section of the steady-state tape-guide spacing, h, for different tape widths at $x = L_x/2$. See the right-hand side column of Table 2 for problem parameters.

The Effect of Axial Tension Variation. In a magnetic recording application the tape tension, T_x, is rarely uniform across the width of the tape. Among the common causes of this non-uniformity is the imperfections in the alignment of guide pins. Another cause of nonuniform axial tension is the driving belts that are used in some tape systems. In Fig. 7 we show two hypothetical axial tension variation cases. In the first case the tension variation is given as follows:

$$T_x(y) = \left(0.6\,\frac{y}{L_y} + 0.7\right)\bar{T}_x \tag{24}$$

where $\bar{T}_x = 276.7$ N/m. This equation provides a 60 percent linear tension increase between the two free edges of the tape. The steady state tape-guide separation, and the corresponding air pressure are shown on the left-hand-side column of Fig. 7. As expected, we observe in this figure that the separation, h, is smaller on the high tension side of the tape. The air responds to this smaller separation by a considerable increase in the pressure at the low flying side.

The second case of tension variation is given by the following equation,

$$T_x(y) = \begin{cases} \left(-1.2\,\dfrac{y}{L_y} + 0.7\right)\bar{T}_x, & \text{for} \quad 0 \le y \le \dfrac{L_y}{2} \\ \left(1.2\,\dfrac{y}{L_y} + 0.7\right)\bar{T}_x, & \text{for} \quad \dfrac{L_y}{2} \le y \le L_y \end{cases} \tag{25}$$

where $\bar{T}_x = 276.7$ N/m. This function represents a 60 percent tension decrease between the edge of the tape and the middle of the tape, followed by an increase of the same amount from the middle to the other edge. The steady-state results of this simulation are given on the right-hand-side column of Fig. 7. As before, the separation, h, is largest where the tension is lowest. The flat region in the middle of the tape is completely lost. The pressure response is also similar.

The Effect of Guide Surface Shape. In many tape cassettes, rigid guide pins are placed in the tape path to make the tape turn a corner. If the conditions of the system are right—in other words, if the radius of the guide is large, and/or the tape tension is low, and/or the tape speed is high—the tape will experience self air lubrication and lift away from the guide surface. This effect is desirable in some tape steering applications because it reduces the driving torque requirements, but it

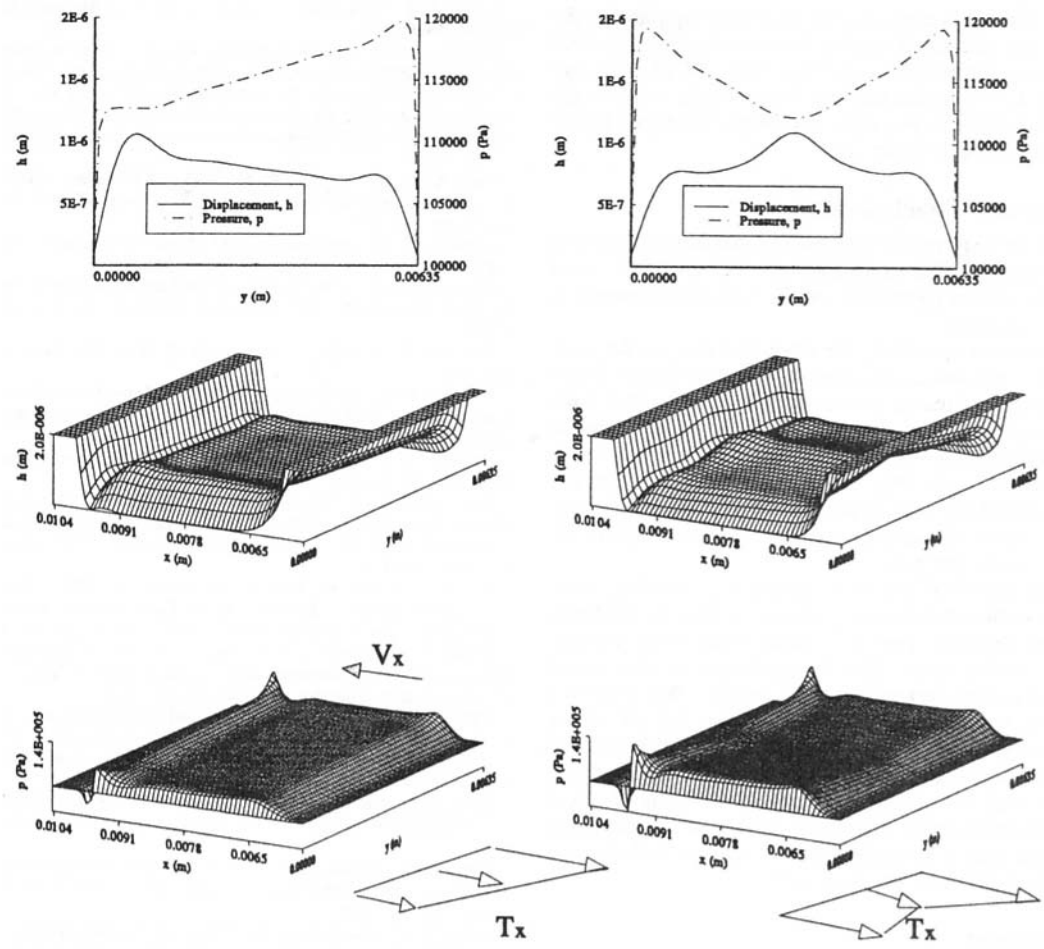

Fig. 7 The effect of axial tension variation on steady state tape-guide spacing, h. Nominal tape tension is T_x = 276.7 N/m, with 30 percent variations as shown. The tape speed and thickness are, V_x = 0.5 m/s, and c = 38.2 μm. See the right-hand side column of Table 2 for other problem parameters.

may be unsatisfactory in other applications if it makes the tape alignment difficult.

Regardless of the intended purpose of the guide, its surface is seldom perfectly straight across the width. In Fig. 8 we show four tape-guide spacings at steady state. The two pictures on the left-hand side column show two surface protrusions with A = 1 and 3 μm amplitudes, and the other two pictures on the right hand side column show two cases of dented surfaces with the same amplitudes. The guide surfaces are also drawn beneath the sketches of the tapes to enable better visualization of the situation. For the parameters that we used in this analysis (Table 2) A = 3 μm is the biggest amplitude that allows complete air bearing

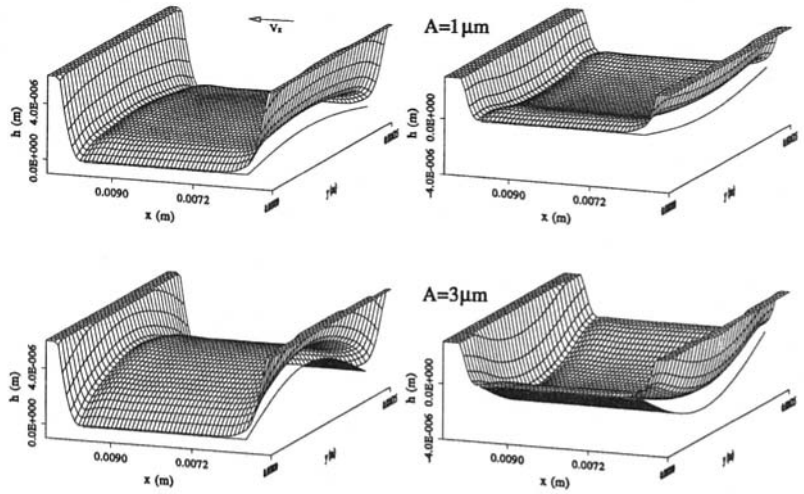

Fig. 8 The effect of axial guide shape on the steady-state tape-guide separation. The guide shape is defined in the axial direction by, A sin ($\pi y/L_y$). See the right-hand side column of Table 2 for problem parameters.

support of the tape. This suggests that for bigger amplitudes the support of the tape due to air bearing becomes harder. The head tape separations at the middle of the tape, $((L_x/2), (L_y/2))$, are given in Table 1. We notice that the flying height is generally higher for dented surfaces. For these parameters the flying height for a flat guide surface is 0.785 μm.

6 Summary and Conclusions

In this paper we analyzed the foil bearing problem in magnetic recording applications. We considered the effects of the axial variations of the system parameters on the tape displacements in the tape-guide interface.

For the parameters studied, we observed that as we consider narrower tapes the displacement boundary layers forming on the lateral edges of the tape mix and the flat zone in the cross-tape direction diminishes. Nonuniform tension variations in the cross-width direction also affect the flatness of the mid-section of the tape. These nonuniformities of the flying height could have an important impact on multichannel recording since the quality of the magnetic signal depends on the head-tape gap.

Our simulations showed that the tape is supported by rigid body contact on the lateral edges where we saw no evidence of air bearing support. The maximum rigid body contact occurs at the exit corners. The flying height at the lateral edges is close to the surface asperity height. We observed that this flying height stays nearly the same for all of the tape speeds, tape tensions we considered. The existence of relatively high contact pressures at the lateral edges make both the tape and the guides vulnerable to wear at these locations. Our simulations also showed that in the case that a guide surface has a sinusoidal protrusion or a dent tape guide separation can still be achieved.

Acknowledgments

Supercomputer time provided by the Laboratory for Laser Energetics of the University of Rochester is greatly appreciated.

References

Barlow, E. J., July, 1967, "Derivation of Governing Equations for Self Acting Foil Bearing," ASME JOURNAL OF LUBRICATION TECHNOLOGY, pp. 334–340.

Bhushan, B., 1990, *Tribology and Mechanics of Magnetic Storage Devices,* Springer-Verlag, NY.

Eshel, A., 1969, "The Propagation of Disturbances in the Infinitely Wide Foil Bearing," ASME JOURNAL OF LUBRICATION TECHNOLOGY, Vol. 91, p. 120.

Fujimoto, K., Nagaoka, E., Watanabe, S., and Kawakami, K., 1993, "Tape Deformation Analysis Considering In-Plane Stress," *Proceedings of the 1993 JSME International Conference on Advanced Mechatronics,* Tokyo, Japan, Aug., pp. 905–910.

Fung, Y. C., and Wittrick, W. H., 1955, "A Boundary Layer Phenomenon in the Large Deflexion of Thin Plates," *Quart. Journ. Mech. and Applied Math.,* Vol. 8, pp. 191–210.

Granzow, G. D., and Lebeck, A. O., 1984, "An Improved One-Dimensional Foil Bearing Solution," ASLE, SP-16, pp. 54–58.

Greenberg, H. J., 1979, "Study of Head-Tape Interaction in High Speed Rotating Head Recording," *IBM Journal of Research and Development,* Vol. 23, p. 197.

Hamrock, B. J., 1994, *Fundamentals of Fluid Film Lubrication,* McGraw-Hill, NY.

Heinrich, J. C., and Connolly, D., 1992, "Three-Dimensional Finite Element Analysis of Self-Acting Foil Bearings," *Computer Methods in Applied Mechanics and Engineering,* Vol. 100, pp. 31–43.

Hughes, T. J. R., 1987, *The Finite Element Method; Linear Static and Dynamic Finite Element Analysis,* Prentice-Hall, NJ.

Kotera, H., Kita, H., Mizoh, Y., and Yohda, H., 1993, "Finite Element Analysis of visco-elastic Frictional Phenomena in VTR," Private communication.

Lacey, C. A., 1992, "The Head/Tape Interface," PhD. thesis, University of California, San Diego.

Mizoh, Y., Yohda, H., Kita, H., and Kotera, H., 1992, "Simulation of Head Wear and Reproduction Envelope by the Finite Element Method," *Electronics and Communications in Japan,* Part 2, Vol. 75, no. 11, pp. 91–100.

Müftü, S., and Benson, R. C., 1994a, "A Numerical Solution for the Transient Displacement of a Circumferentially Moving Cylindrical Shell," ASME *Journal of Vibration and Acoustics,* Vol. 116, pp. 567–572.

Müftü, S., 1994b, "The Transient Foil Bearing Problem in Magnetic Recording," Ph. D. Thesis, University of Rochester, Rochester, NY.

Rongen, P. M. J., 1990, "On Numerical Solutions of the Instationary 2D foil Bearing Problem," ASLE SP-29, pp. 130–138.

Stahl, K. J., White, J. W., and Deckert, K. L., 1974, "Dynamic Response of Self Acting Foil Bearings," *IBM Journal of Research and Development,* pp. 513–520.

Vogel, S. M., and Groom, J. L., 1974, "White Light Interferometry of Elastohydrodynamic Lubrication of Foil Bearings," *IBM Journal of Research and Development,* pp. 521–528.

White, J. W., and Nigam, A., 1980, "A Factored Implicit Scheme for the Numerical Solution of the Reynolds Equation at Very Low Spacing," ASME JOURNAL OF LUBRICATION TECHNOLOGY, Vol. 102, pp. 80–85.

Wolf, B., Deshpande, N., and Castelli, V., 1983, "The Flight of Finite Width Foil Bearings," ASME JOURNAL OF LUBRICATION TECHNOLOGY, Vol. 105, pp. 138–142.

Yoneda, K., and Sawada, T., 1988, "Simulation of Tape Flying Characteristics Above VTR Drum Considering In-Plane Stresses," *IEEE,* No. 6, Vol. 24, pp. 2766–2768.